Evaluation of ISCCP Multisatellite Radiance Calibration for Geostationary Imager Visible Channels Using the Moon

Thomas C. Stone, William B. Rossow, Joseph Ferrier, and Laura M. Hinkelman

***Abstract*—Since 1983, the International Satellite Cloud Climatology Project (ISCCP) has collected Earth radiance data from the succession of geostationary and polar-orbiting meteorological satellites operated by weather agencies worldwide. Meeting the ISCCP goals of global coverage and decade-length time scales requires consistent and stable calibration of the participating satellites. For the geostationary imager visible channels, ISCCP calibration provides regular periodic updates from regressions of radiances measured from coincident and collocated observations taken by Advanced Very High Resolution Radiometer instruments. As an independent check of the temporal stability and intersatellite consistency of ISCCP calibrations, we have applied lunar calibration techniques to geostationary imager visible channels using images of the Moon found in the ISCCP data archive. Lunar calibration enables using the reflected light from the Moon as a stable and consistent radiometric reference. Although the technique has general applicability, limitations of the archived image data have restricted the current study to Geostationary Operational Environmental Satellite and Geostationary Meteorological Satellite series. The results of this lunar analysis confirm that ISCCP calibration exhibits negligible temporal trends in sensor response but have revealed apparent relative biases between the satellites at various levels. However, these biases amount to differences of only a few percent in measured absolute reflectances. Since the lunar analysis examines only the lower end of the radiance range, the results suggest that the ISCCP calibration regression approach does not precisely determine the intercept or the zero-radiance response level. We discuss the impact of these findings on the development of consistent calibration for multisatellite global data sets.**

***Index Terms*—Calibration, Moon, radiometry, remote sensing.**

Manuscript received January 30, 2012; revised June 11, 2012 and November 19, 2012; accepted December 16, 2012. Date of current version February 21, 2013. This work was supported in part by the National Aeronautics and Space Administration (NASA) Earth Science Research Program under Interagency Agreement NNX08AJ80G and in part by the NASA Earth Science Data Systems Making Earth System Data Records for Use in Research Environments Program under Contract NNX08AL79A.

T. C. Stone is with the Astrogeology Science Center, U.S. Geological Survey, Flagstaff, AZ 86001 USA (e-mail: tstone@usgs.gov).

W. B. Rossow is with The City University of New York, New York, NY 10031 USA (e-mail: wbrossow@ccny.cuny.edu).

J. Ferrier is with the Goddard Institute for Space Studies, National Aeronautics and Space Administration, New York, NY 10025 USA (e-mail: joe@ferrier.com).

L. M. Hinkelman is with the Joint Institute for the Study of the Atmosphere and Ocean, University of Washington, Seattle, WA 98195 USA (e-mail: laurahin@u.washington.edu).

Digital Object Identifier 10.1109/TGRS.2012.2237520

I. Introduction

FROM its inception, the International Satellite Cloud Climatology Project (ISCCP) [1] has addressed the many challenges of assembling long-term global-coverage data sets from observations taken by multiple instruments on different satellite platforms. Meeting these needs has assumed a greater significance as the imperative of measuring climate variables and detecting climate change has become a driver for Earth-observing satellite missions. In successfully treating the complications of interoperability of observational data sets from different platforms and operation agencies, the ISCCP collection of global radiance and cloud data products has established many precedents for the development of climate data records. For example, ISCCP produced the first instance where the global constellation of weather satellites has been calibrated to a common standard.

The overall objective of ISCCP is to enable study of the effects of clouds on geophysical processes by providing quantitative information on the spatial and temporal variations of cloud radiative properties at spatial scales from regional to global and temporal scales from diurnal to decadal. This has been accomplished by combining observations from both geostationary and polar-orbiting satellites, taking advantage of the continuity offered by series of meteorological satellites. Since 1983, ISCCP has collected radiance data acquired by the imaging radiometers of the world's meteorological agencies: the U.S. National Oceanic and Atmospheric Administration (NOAA), the European Organisation for the Exploitation of Meteorological Satellites (EUMETSAT), the Japan Meteorological Agency (JMA), and the China Meteorological Administration (CMA). The polar orbiters include NOAA-7 through NOAA-18, NOAA-13 excepted. The geostationary satellites include Geostationary Operational Environmental Satellite GOES-5 through GOES-13 (NOAA); Meteosat-2 through Meteosat-9 (EUMETSAT); Geostationary Meteorological Satellite GMS-1 through GMS-5, Multifunctional Transport Satellite MTSAT-1R, and MTSAT-2 (JMA); and Fengyun FY-2C and FY-2E (CMA).[1]

Combining observational data from the meteorological imagers of multiple weather agencies into a consistent global data set requires that the sensors be calibrated to a common radiometric scale. For climate studies, the calibration must

[1]The Indian Space Research Organisation contributed about 11 months of data from Indian National Satellite INSAT-1B in the late 1980s.

be maintained over time scales that exceed typical satellite lifetimes. To utilize such a data set for assessing the physical attributes of clouds from their measured radiances requires absolute calibration. Historically, the visible-channel imagers on meteorological satellites have not been equipped with onboard calibration systems. Quantitative radiometric calibration therefore must rely on external reference sources and applications of vicarious calibration (e.g., [2]–[4]) and other special techniques.

The ISCCP calibration concept for visible wavelengths involves referencing the geostationary imagers to polar-orbiting radiometers that underfly them, maintaining calibration of the reference polar instruments over their lifetimes and across the succession of satellites, and tying the absolute scale to vicarious calibration measurements [5]–[7]. Although many meteorological instruments have several spectral bands, ISCCP calibration procedures focus on the only two bands common to all weather satellites: a visible wavelength (VIS) channel at ~ 0.6 μm and a "window infrared" wavelength channel at ~ 11 μm.

The reference for ISCCP VIS calibration derives from the Advanced Very High Resolution Radiometer (AVHRR) on NOAA-9. The procedure is described in detail in [5] and [7]. The absolute scale for this reference radiometer was established from simultaneous and coincident measurements taken by a calibrated spectrometer on a series of National Aeronautics and Space Administration (NASA) ER-2 aircraft underflights. The NOAA-9 AVHRR was determined to be the best-calibrated instrument used by ISCCP, given the extensive efforts devoted to its calibration by several groups [8]–[10]. Uncertainty in the calibration developed by this method is estimated to be 5%–10% absolute [7], primarily due to the uncertainty in individual aircraft measurements [11].

Calibration stability and consistency are realized through analysis of AVHRR radiance measurements found in the ISCCP data set, using a variety of targets consisting of nine different land surface types and the entire globe as a target. Radiance histograms for the target data are used for filtering to select only clear-sky conditions, and the (filtered) global mean radiances for these targets are presumed constant on an annual time scale. The method provides for linear degradation trending for each AVHRR and for transfer of the NOAA-9 reference calibration to successor and predecessor radiometers. Each instrument is corrected for drift using an iterative process that produces a zero trend in the mean surface visible reflectance over the lifetime of each satellite, aligns the calibrations at the satellite crossover points, and adjusts the absolute scale to the NOAA-9 reference. Taking the uncertainties of these steps together, ISCCP has determined that the VIS calibration relative uncertainty is no larger than $\pm 3\%$–5% over the entire radiance data set [7].

Transfer of the reference calibration to the geostationary imagers involves comparisons of radiances from a distribution of targets near the geostationary subsatellite point that are coincident and collocated with the polar orbiter radiometer data. Details of the procedure are found in [6]. Geostationary and polar orbiter images are chosen with the closest available acquisition time, but not more than 10-min difference, to assure that the targets have nearly identical illumination and viewing geometry; typically, five coincident images are used in each radiance comparison. Target sample areas of about 50 km $\times$ 50 km are identified at 10 to 20 locations per image, and quality checks are conducted based on the radiance distribution within these areas to emphasize scene homogeneity. To minimize the effects of spectral response differences in the VIS imagers, targets are restricted to clear ocean and clouds over ocean, although bright clouds over land are sometimes used when necessary. These targets are considered representative of the instruments' response to radiation with the same spectral distribution as the Sun. All acceptable coincident data acquired over a month are used in least squares linear regressions of the polar radiometric measurements against the geostationary radiometric measurements. A linear fit of radiance to radiance produces a normalization slope and an intercept. Initially, this normalization process was conducted every three months, with linear interpolation of the results to the intervening periods. With a revision of the ISCCP calibration procedures implemented after examination of about ten years of radiance data [7], normalization is now performed monthly. This approach accounts for changes in the geostationary sensors' radiometric response at the time scale of these periodic updates.

In preparation for the next major reprocessing of the ISCCP data set, calibration of the VIS-channel radiometers has been revisited. Techniques developed for NASA's Earth Observing System program to realize in-flight calibration of satellite instruments have been applied to archived ISCCP data with the goal of assessing the accuracy and consistency of the radiance data set.

This paper describes a study of the ISCCP VIS-channel calibration for geostationary satellites through application of lunar calibration techniques. A methodology that enables the Moon to be used as a stable radiometric reference source at reflected solar wavelengths has been developed by the U.S. Geological Survey (USGS) in Flagstaff, AZ [12]. The Moon regularly passes through the view field of geostationary satellite imagers, and lunar images periodically are captured in the space-viewing corners and margins of a typical rectangular field of regard. Although favorable geometries for Moon observations from geostationary orbit occur several times per month, the number of Moon images captured by chance in the ISCCP archive is limited by the 3-h sampling frequency of the collection. Nonetheless, a sufficient number of observations have been found to derive meaningful results from lunar calibration analysis. The current study has evaluated the multiyear (decadal time scale) multisatellite ISCCP calibration against an independent common standard, the Moon.

Section II describes the procedures for selection and subsampling of full-disk images that contain the Moon and the steps for processing these image data for application of lunar calibration. Section III develops radiometric comparisons of the Moon measurements taken by the geostationary instruments against the USGS lunar model reference, and Section IV examines the results. Section V provides an assessment of the uncertainties involved with the techniques applied here and an evaluation of the ISCCP radiance calibration in the context of this lunar calibration analysis. Section VI concludes this paper by discussing the findings of this study in the context of a multisatellite, consistent calibration effort and the larger

implications for developing global data sets with climate-quality calibration.

II. Lunar Image Data and Processing

The USGS lunar calibration system operates with the radiometric quantity of spatially integrated lunar spectral irradiance, comparing measurements derived from observations of the Moon made by instruments against computations of a lunar spectral irradiance model [12] for the particular conditions of the instrument observations. Processing of radiance (image) data to irradiance involves summation of image pixels that constitute the lunar disk, accounting for spatial oversampling and subtracting the sensor background response. The latter is a particularly sensitive process because the Moon is a relatively dark target, with a disk-averaged reflectance around 0.11, although this quantity is highly dependent on phase angle and wavelength.

Because lunar irradiance measurements are sensitive to the selection of pixels that constitute the lunar disk, it is desirable to work with the highest spatial resolution data available. To meet an initial challenge of managing large quantities of meteorological image data, ISCCP developed a spatial sampling scheme for VIS-channel data in which full-resolution image pixels are averaged to match the footprint size of the infrared-channel pixels; then, these average pixels are subsampled at $\sim$10-km intervals. The ISCCP archive retains image data at this level of processing, called stage B1 [13], at 3-h imaging intervals. At the start of data collection in 1983, ISCCP archiving systems used nine-track tape media. To keep physical storage requirements to a manageable size, the full-resolution raw images collected by ISCCP (called stage A) were not saved. In some cases, the ISCCP B1 archive may be the only remaining record of historical meteorological images at a low processing level (e.g., raw sensor output) for the earliest satellites.

Recently, the NOAA National Climatic Data Center (NCDC) has undertaken recovery of the ISCCP B1 data from the tapes to an updated archiving system [14], with the goals of preserving and improving the interoperability of data from the different ISCCP processing centers. A new B1 unified (B1U) format was developed under this program. The current study used these B1U format data exclusively.

A. Image Selection and Subsampling

Determining which images in the ISCCP archive might contain the Moon involves predicting the relative geometry that finds the Moon in a position to appear within the view field of the geostationary imagers. The absolute position of the Moon in Earth-centered inertial coordinates can be predicted with high accuracy from ephemeris computations. This study utilized the DE421 ephemeris available from the NASA Jet Propulsion Laboratory (ftp://ssd.jpl.nasa.gov/pub/eph/planets). The position of the geostationary satellites was determined by propagating their orbits to the times of possible Moon appearances using two-line orbital element (TLE) sets available from Space Track (http://www.space-track.org). However, the satellite positions computed from TLE were found to lack sufficient accuracy to predict the precise location of the lunar disk in a full-Earth image. Therefore, the geometric criteria for asserting whether the Moon possibly is in an image field had to be loosened, resulting in an increased number of "false positive" predictions.

ISCCP B1U filenames are constructed to contain the nominal image start time. A filename list of all archived B1U files was parsed to extract the start times, for comparison against the predicted times when the Moon is in view. The filenames corresponding to potential Moon image captures were submitted to NOAA NCDC to obtain the B1U data.

For each image possibly containing the Moon, the relative view geometry was computed for each scan line using the line timestamps recorded in the B1U data headers. Where line timestamps were not available, scan timings were inferred from operational specifications of the instruments. This procedure can detect the presence of the Moon within the accuracy of the satellite absolute position computations. At the radius of geostationary orbit (42 164 km), a 500-km error in the predicted satellite position translates to an offset in the Moon image location of $\sim$10.7 millirad (for reference, the Moon diameter is about 8 millirad). Our experience suggests that errors in the orbit predictions from TLE can be considerably larger than this. Therefore, actual determination of the presence of the Moon required interactively viewing the images. For those images in which the Moon appears, subframes were extracted using rectangular framing areas and saved in a 120 $\times$ 120 pixel format. At the spatial resolution of ISCCP B1 data, the Moon's disk is about 35–40 pixels in diameter. The larger subframe dimensions were chosen to accommodate highly elongated framing areas, which can be necessary to avoid scattered light from the Earth limb and/or proximity of the Moon image to the full-frame edges, while including sufficient space-viewing pixels surrounding the Moon.

Fig. 1(a) shows an example ISCCP B1 Moon image acquired by GOES-10 on August 9, 1998, at 21:00 Coordinated Universal Time (UTC). The phase angle is 23.5°, and the lunar disk is about 95% illuminated. The disk appears skewed due to the construction of geostationary images from sequential scan lines, where the orbital motion of the satellite during the scan intervals induces a horizontal offset in the apparent position of the Moon with each line.

B. Lunar Irradiance Processing

The lunar irradiance E measured from radiance images of the Moon is found by spatial integration of pixels

$$E = \Omega_{\mathrm{pix}} \sum_{i=1}^{N} L_i \tag{1}$$

where Ω_{pix} is the solid angle subtended by one pixel, L_i is the radiance measure of pixel i, and the summation covers all pixels on the lunar disk N. Pixel solid angles typically are computed from the native spatial (angular) resolution of an imager sensor. For ISCCP B1 data, the spatial resolution must be scaled by the B1 subsampling factors; these parameters are tabulated for all satellites used by ISCCP [15] and usually can

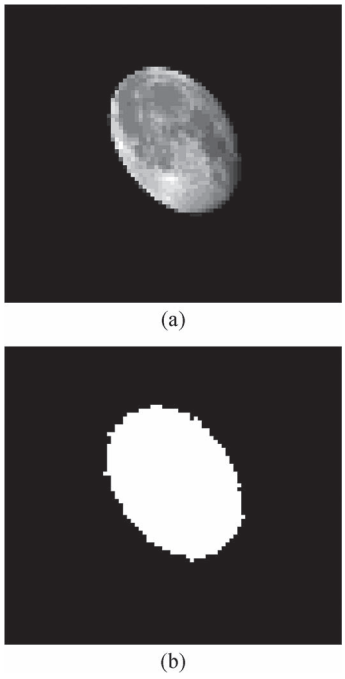

Fig. 1. (a) GOES-10 image of the Moon in ISCCP B1 data, acquired on August 9, 1998, at 21:00 UTC. (b) Corresponding image processing pixel mask, for selection of on-Moon pixels.

be found in the B1U data headers. In some cases, ISCCP stage-A image pixels differ from the sensor native resolution, notably for Meteosat, where the level-1.5 images used as stage A have been reprojected from native level-1.0 images.

A variety of methods exist for selection of the on-Moon pixels, and the choice can be somewhat subjective. The selection algorithm developed for this study applies a threshold test on pixel brightness level, accepting pixels that exceed a specified threshold above the dark (space-view) level and also including pixels within a user-specified spatial proximity to the above-threshold pixels. Fig. 1(b) shows the mask indicating the on-Moon pixel selection for the image in Fig. 1(a).

The dark response level for each lunar subframe is determined from the maximum of the histogram of the subframe, as space-view pixels form the largest, most narrowly distributed pixel group. All ISCCP B1 image data have 8-b depth; data from sensors having other native dynamic ranges (such as the 10-b GOES sensors) have been scaled to 8-b depth. Dark levels were typically found to be ~7–8 digital data numbers (DN) or *counts* (CT), although this varies among the different sensors. The threshold for on-Moon selection was chosen as 2 DN above the dark level. The proximity selection applies a nearest neighbor test in all directions to add pixels within a specified spatial range of the threshold-selected pixels, while also deselecting isolated above-threshold pixels. The proximity value was chosen as two pixels. Both these parameter choices were based on consistency checks on a substantial number of test irradiance summations. Pixels falling below the threshold value and outside the proximity boundary are designated as space view; however, additional checks are performed on both the on-Moon and space-view ensembles to cull anomalously high- or low-valued pixels. This pixel selection method was chosen to accommodate the irregular lunar disk shapes resulting from the geostationary image construction from sequential scans, exacerbated by the ISCCP B1 subsampling scheme, which makes the images not well suited for delineating the disk of the Moon based on its expected shape, such as fitting an ellipse to the high-contrast transition region from the bright limb to space. Use of this chosen method may increase the uncertainty in the irradiance measurements; this is discussed in Section IV-B.

The B1 image pixel values in counts (CT), are converted to radiance units (in watts per square meter per steradian) utilizing the ISCCP radiometric calibration tables, called BT [15]. The BT absolute radiance tables are provided in the headers of B1U image files, but these header data must be checked against the most recent BT products generated by ISCCP (available at the ISCCP Web site: http://isccp.giss.nasa.gov), as these may be updated by changes made during cloud product generation. Since the lunar calibration system works with spectral irradiance, the imager spectral response functions are accounted for in the radiance conversion by dividing by the band equivalent width.

Space-based sensor systems typically are designed with a small bias applied in the analog signal chain to give a positive output value for zero-radiance input. This offset must be evaluated and subtracted from the image data to compute absolute radiance. The threshold/proximity pixel selection algorithm described above also identifies space-view pixels that are contaminated by stray light (e.g., scattering from the illuminated Earth) and transient detector anomalies based on extreme excursions from a normal distribution of counts. The mean value of the "good" space-view pixels $\mathrm{CT}_{\mathrm{sp}}$ has been used here to determine the sensor bias offset.

As a measure to conserve downlink bandwidth and increase sensor dynamic range, some geostationary imagers applied quadratic signal processing to the sensor output, making the measured radiance proportional to counts squared (CT^2). The imagers used in this study with quadratic response are on GOES-6, GOES-7, and GMS-3 through GMS-5. Thus, two forms were needed for the pixel radiance conversions. For processing that measures the sensor bias offset from space-view pixels

$$L_i = S_a \cdot (\mathrm{CT}_i - \mathrm{CT}_{\mathrm{sp}})/\Delta\lambda_{\mathrm{eq}} \quad \text{or}$$
$$L_i = S_a \cdot \left(\mathrm{CT}_i^2 - \mathrm{CT}_{\mathrm{sp}}^2\right)/\Delta\lambda_{\mathrm{eq}} \tag{2}$$

where S_a is the ISCCP absolute calibration slope from the BT tables and $\Delta\lambda_{\mathrm{eq}}$ is the band equivalent width. Alternatively, the ISCCP calibration was used directly in its slope–intercept form

$$L_i = (S_a \cdot \mathrm{CT}_i + I_a)/\Delta\lambda_{\mathrm{eq}} \quad \text{or}$$
$$L_i = \left(S_a \cdot \mathrm{CT}_i^2 + I_a\right)/\Delta\lambda_{\mathrm{eq}} \tag{3}$$

where I_a is the ISCCP absolute calibration intercept obtained from the BT tables. Both calibration methods were applied to the lunar data sets used in this study; the differences in results are discussed in Section IV-C.

Lastly, obtaining absolute lunar irradiance measurements from pixel summations of ISCCP B1 image data requires an areal correction for the spatial subsampling performed during processing to stage B1. The subsampling factors typically are

provided in the B1U data headers. Scaling by these factors in effect reverts the spatial sampling to ISCCP stage-A resolution and thus includes any image oversampling. Oversampling factors are not provided in B1U header data and therefore must be obtained from operational specifications for each satellite. For the imagers used in this study, the factors are as follows: 1.106 for GOES-6 and GOES-7, 1.75 for GOES-8 through GOES-12, and 1.460 for GMS-3 through GMS-5.

III. Comparisons to the Lunar Irradiance Model

The USGS lunar calibration facility provides the radiometric reference of the Moon as the lunar spectral irradiance, generated by a numerical model that was developed from extensive ground-based observations [12]. The model has an empirically derived analytic form, with a continuous predictive capability that can accommodate any views of the Moon taken by Earth-orbiting instruments without restrictions on observation time or geometry. Standardized model outputs are adjusted for the specific conditions of the instrument observations, enabling direct comparisons of the measured and modeled lunar irradiances.

A. Model Operation, Input, and Output

Operationally, the USGS lunar model generates spectral irradiance from the lunar disk-equivalent reflectance. The conversion between irradiance and reflectance involves a solar spectral model; however, the influence of the particular solar model used is a second-order effect if a consistent choice is maintained for both lunar model development and operation.

Considering a view of the Moon taken from the vantage point of an Earth-orbiting spacecraft, the (monochromatic) spatially integrated lunar disk reflectance is a function of only the phase angle and the particular hemispheres of the Moon that are illuminated and viewed. The latter define the lunar librations and are specified by the subsolar and subobserver coordinates on the lunar surface. Accordingly, the lunar reflectance model operates with only the geometric variables of phase angle, observer selenographic longitude and latitude, and solar selenographic longitude (during model development at USGS, the dependence on solar selenographic latitude was found to be negligible). Details are found in [12].

In practice, the external inputs provided to the USGS lunar calibration system are the ephemeris time of a Moon observation and the instrument location at this time. The geometric variables actually supplied to the numerical model (phase and libration) are developed within the system by ephemeris computations and coordinate transformations. Additional required inputs are the instrument-measured irradiance and the image oversampling factor, plus the instrument band spectral response for initial system setup.

For this ISCCP study, the Moon observation times were defined by the scan line passing through the widest part of the lunar disk image, determined during extraction of the subframes from the full-disk images. The satellite location was found by propagating the orbit to the observation time using the appropriate TLE set. The imager spectral response functions were obtained from the ISCCP archive, originally provided by the various satellite operators.

For a given set of phase and libration inputs, the lunar model generates the disk-equivalent reflectance at 32 discrete wavelengths. These values are interpolated to the instrument bands along a representative lunar reflectance spectrum and then converted to spectral irradiance at each band wavelength.

The irradiance quantity varies with both Sun–Moon and Moon–observer distances as the inverse square of the distances. The basic model computations correspond to the "standard" distances of the mean orbital radii of the Earth and Moon, i.e., 1 AU and 384 400 km, respectively. Corrections to the actual observation distances are applied to the model outputs, making the model irradiances directly comparable to the instrument measurements. These results are reported as the (relative) discrepancy δ in percent between the measured and modeled irradiances

$$\delta = \left(\frac{\text{measured}}{\text{model}} - 1 \right) \times 100\%. \tag{4}$$

This discrepancy quantity is used hereafter for presentation of the lunar calibration results.

B. Application to ISCCP Geostationary Imagers

While conducting the initial procedures for finding Moon images in the ISCCP geostationary archive (cf. Section II-A), some notable exceptions were discovered. Since ISCCP B1 data for the Meteosat imagers are derived from Meteosat level-1.5 images, all off-Earth pixels (where the Moon can appear) are nulled. Similar treatment was found for MTSAT-1R data. This precluded these instruments from being used in this study. However, full-resolution Meteosat level-1.0 data, in which all pixels in the field are preserved, are available from the EUMETSAT Data Centre archive (http://archive.eumetsat.int). Thus, it is possible to apply lunar calibration analysis to Meteosat imagers using EUMETSAT data, and this is being done under a separate study. For the B1 image data that retained the off-Earth pixels, a small number of Moon images were found to be either clipped by the image frame or occulted by the Earth. Also, the lunar irradiance processing in this study utilized the most current ISCCP BT calibration tables, obtained from either the B1U data headers or the ISCCP archive. Less than complete availability of these tables has somewhat limited the time period for possible analysis, particularly for the earlier satellites, and has excluded FY-2C and FY-2E. Table I lists the satellites used in this study, with the dates for the earliest and latest usable Moon images found and the number of images used.

Figs. 2–4 show time series of lunar irradiance comparisons for the GOES and GMS series listed in Table I. The plot ordinates are the discrepancies in percent between measured and modeled irradiance values, per (4). The open symbols correspond to images where (2) was used for pixel radiance conversion, where the calibration slope S_a was obtained from the image header table and the space-level count value $\mathrm{CT_{sp}}$ was determined from the mean of space-view pixels, for example, the dark regions in Fig. 1(b). The filled symbols indicate

TABLE I
INCLUSIVE DATES FOR ISCCP GEOSTATIONARY IMAGES USABLE FOR LUNAR CALIBRATION ANALYSIS

Satellite	First Date	Last Date	Number of Moon Images
GOES–6	1983-08-01	1988-05-24	17
GOES–7	1988-02-07	1995-10-04	22
GOES–8	1995-06-08	2003-02-20	27
GOES–9	1996-03-31	1998-04-12	7
GOES–10	1998-08-09	2006-03-13	22
GOES–11	2007-01-08	2008-05-15	5
GOES–12	2003-04-14	2008-04-18	13
GMS–3	1984-12-04	1989-02-21	7
GMS–4	1990-10-04	1995-04-10	11
GMS–5	1995-09-12	2003-01-22	22

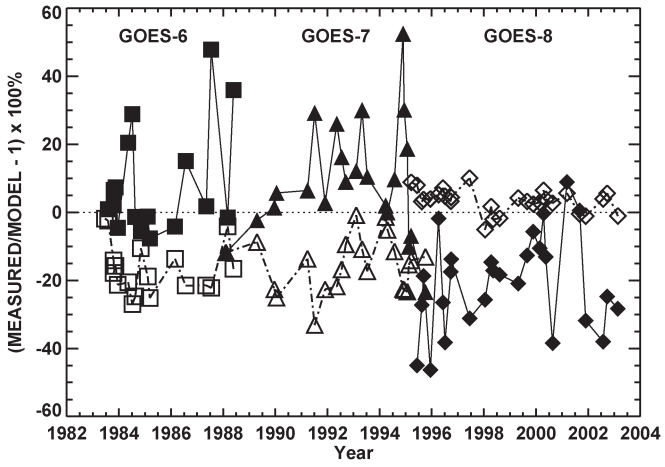

Fig. 2. Time series of lunar irradiance comparisons for GOES-6, GOES-7, and GOES-8, given as percent difference from the USGS lunar model (4). Data points show all usable Moon images found in the ISCCP B1U archive (see Table I). Open symbols with broken connecting lines indicate pixel radiance conversion using (2); filled symbols indicate ISCCP calibration conversion (3). (Squares) GOES-6. (Triangles) GOES-7. (Diamonds) GOES-8.

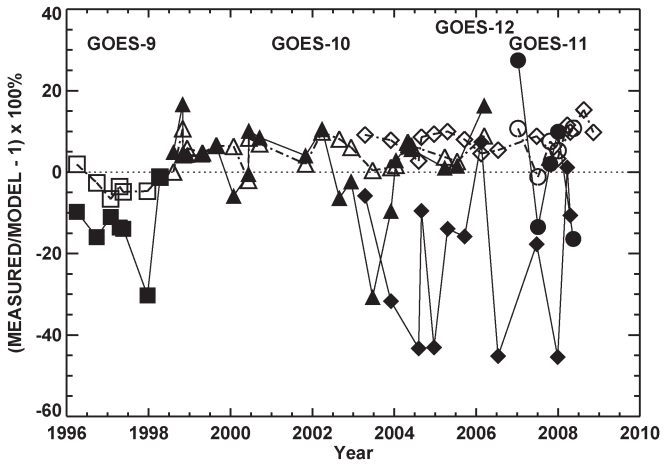

Fig. 3. Time series of lunar irradiance comparisons for GOES-9 through GOES-12, given as percent difference from the USGS lunar model (4). Data points show all usable Moon images found in the ISCCP B1U archive (see Table I). Open symbols with broken connecting lines indicate pixel radiance conversion using (2); filled symbols indicate ISCCP calibration conversion (3). (Squares) GOES-9. (Triangles) GOES-10. (Circles) GOES-11. (Diamonds) GOES-12.

data points where the ISCCP slope–intercept form of radiance conversion (3) was applied, using intercept values from the archived ISCCP BT calibration tables appropriate for each

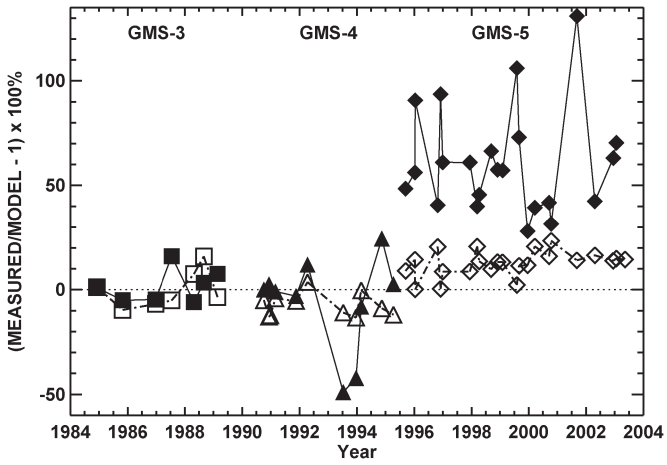

Fig. 4. Time series of lunar irradiance comparisons for GMS-3, GMS-4, and GMS-5, given as percent difference from the USGS lunar model (4). Data points show all usable Moon images found in the ISCCP B1U archive (see Table I). Open symbols with broken connecting lines indicate pixel radiance conversion using (2); filled symbols indicate ISCCP calibration conversion (3). (Squares) GMS-3. (Triangles) GMS-4. (Diamonds) GMS-5.

image. The connecting lines are provided as visual aids, to discriminate the different satellite series.

IV. DISCUSSION

Comparing lunar irradiance measurements to model results using (4) effectively normalizes the observed variations in the lunar brightness with phase angle and librations. The lunar data set represented by the list in Table I ranges in phase angle from $\sim 4^\circ$ to $\sim 90^\circ$, and the corresponding lunar irradiances vary by more than an order of magnitude.

Each data point in Figs. 2–4 represents a quantitative evaluation of sensor response compared against the lunar reference, in the form of the USGS lunar irradiance model. The model irradiance predictions are self-consistent with a relative precision better than 1% [12] for a given sensor for any phase angle within the valid range $\pm 90^\circ$, where negative numbers signify waxing lunar phases. This high level of precision enables informative analysis by considering the series of lunar comparison results taken collectively for each satellite.

A. Time Series Scatter

All the current series of irradiance comparisons show scatter considerably greater than the lunar model's internal consistency, regardless of any systematic biases attributable to error in the model absolute scale (cf. Section V-A). The relation of this scatter to sensor calibration uncertainty is discussed in Section V-C. The high relative precision of the lunar model predictions means that the model computations themselves contribute minimally to the scatter. This can be demonstrated by generating lunar reflectance phase curves from both the model results and the instrument measurements. A typical example is shown in Fig. 5 for the GOES-8 series. For the instrument-derived values, the lunar disk reflectance A can be computed from the irradiance measurements $E_{\rm meas}$ (1) by

$$A = \frac{\pi\, E_{\rm meas}}{\Omega_M\, E_{\rm Sun}} f_d \tag{5}$$

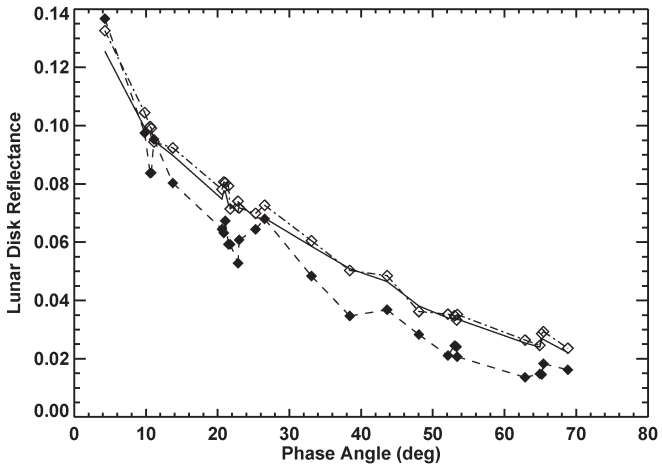

Fig. 5. Lunar disk reflectance phase curves for the GOES-8 series. Model results are shown as a solid line; symbols indicate reflectances computed from measurements using (5), with pixel radiance conversion by (open symbols) (2) and (filled symbols) (3). Deviations from a smooth curve show the effects of lunar librations.

where E_{Sun} is the solar spectral irradiance at the sensor band wavelength, Ω_M is the solid angle of the Moon at the spacecraft observation location, and f_d is the correction factor to normalize the Sun–Moon distance. The fundamental lunar model computations are the disk-equivalent reflectance at the standard distances (1 AU and 384 400 km). The lunar reflectance phase curve is generally known to be a smooth function at any wavelength. The small variations seen in the model results (solid line) are due to the effects of the lunar librations, and corresponding structure is expected and observed in the measured reflectances. However, the measurement results vary far more than what can be accounted for by the contributions of the librations.

Therefore, the observed scatter must originate with the irradiance measurements, as calculated using (1). Several potential sources of this scatter have been identified and described here.

On-Moon Pixel Selection: The particular selection of pixels constituting the lunar disk can directly influence the irradiance measurements. Because the same on-Moon pixel mask was used for both methods of radiance conversion [(2) and (3)], any error due to pixel selection should be correlated between the two measurement results. The phase curve plots in Fig. 5 show qualitatively such a correlation. A test study was conducted to examine the effects on the encircled energy measured from the GOES-8 images by incrementally expanding the perimeter of the lunar disk inclusion area. The intent was to capture any response to moonlight that might fall below the threshold of the pixel selection algorithm. An expansion by two pixels in each direction was found to increase the encircled energy (irradiance) typically less than 1%. Rendering the measurements as reflectances, as in Fig. 5, also can reveal any correlation with phase angle, which could be indicative of a systematic pixel selection bias. The phase correlations of the measurement-to-model differences in the GOES-8 phase curves were found to be -0.177 and -0.035. These small correlation values lead us to conclude that the on-Moon pixel selections are adequate and not a source of systematic uncertainty.

B1 Subsampling Errors: As a result of the spatial averaging and subsampling processes used for ISCCP B1 data production (cf. Section II and [13]), B1 images represent only about 40% of the original image area, although this number varies for different satellites. This approach for reducing spatial resolution is acceptable for studies of cloud radiative properties, the primary objective of ISCCP, but the subsampling operation could affect the distribution of radiances obtained from a spatially inhomogeneous target such as the Moon. A quantitative evaluation of the error introduced by the B1 subsampling processing is given in Section V-B.

Background-Level Offset: The sensor response to zero-radiance input influences the lunar irradiance measurements through the pixel radiance conversions, either directly by (2) or indirectly through the intercept of (3). Typically, raw sensor data for dark (zero radiance) targets have a nonzero count value imposed in the onboard signal processing chain. This process, sometimes called the "space clamp", fixes the value (in DN, or counts) of the sensor output when viewing deep space. Contamination from stray light and/or other detector anomalies present during this space view can produce an offset between the fixed (clamp) level and the actual sensor response to zero-radiance input, although the magnitude of such an offset generally cannot be known. Stray light contamination also can skew the normal noise distribution of the sensors' dark response. These effects can introduce uncertainties in the dark-level subtraction of the pixel radiance conversion, and this would disproportionately affect measurements of low-radiance targets such as the Moon. An additional complication for the current study was that the data for GMS-5 were found to have had the zero-radiance count values artificially offset to a zero average, retaining only the positive side of the dark noise distribution. Consequently, statistical analysis of the space-view pixels is inappropriate for these cases, and radiance conversion by (2) required imposing the artificial constraint $\mathrm{CT}_{\mathrm{sp}} = 0.0$.

ISCCP Calibration for Geostationary Imagers: As described in Section I and in the literature [6], [7], the ISCCP calibration method for geostationary imager data involves regression of radiances from ground targets coincident and collocated with AVHRR observations. The intercept values I_a [cf. (3)] obtained by this procedure estimate the zero-radiance response offsets under the assumptions that the reference polar radiometer has an accurate and stable calibration and the geostationary sensors have linear response characteristics. This attribute is not affected by the artificial background level imposed on the GMS-5 B1 data. The current lunar calibration analysis has produced an independent check of these estimates.

The comparison results plotted in Figs. 2–4 show consistently larger scatter when the slope–intercept form (3) is used for pixel radiance conversion (filled symbols). Furthermore, a strong correlation $(r = 0.795)$ was found between these variances and the variations seen in the calibration intercept values. The targets used for ISCCP geostationary calibration are deliberately chosen to bracket a wide range of radiances; thus, the slope fit is much better determined than the intercept. Since the radiances are fitted without constraints on either parameter, the influence of higher valued pixels could be skewing the low-radiance end of the regression, leading to a less precise

specification of the intercept. Nonetheless, these variations in the ISCCP calibration intercept translate to only a few percent error in the absolute measured radiances. Statistical evaluations of the current lunar comparisons are presented in Section IV-C.

B. Temporal Trends

The value of the Moon as a radiometric reference derives from its exceptional temporal stability, estimated at $< 10^{-8}$ per year [16]. Consequently, the lunar irradiance model has no time dependence, and thus, it can be used to cross-compare Moon observations made at any time, regardless of the interval between them. A series of Moon observations normalized by the lunar model can reveal temporal response trends of sensors very effectively.

One of the primary goals for ISCCP data production has been to provide global radiances with temporally stable and consistent calibration across the entire data set. The current lunar calibration results provide a means to verify these attributes. Although the number of chance Moon captures identified in the ISCCP data set was relatively low, enough usable images were found to conduct temporal trend analyses for each of the satellites used in this study. Since ISCCP calibration coefficients were used to develop the lunar irradiance measurements presented here, minimal response trends were expected from the series of lunar model comparisons. The data in Figs. 2–4 were fitted with linear functions of time separately for each satellite, with quantitative uncertainties computed for the fit parameters. In each case, departure from a flat (zero) trend could not be discerned with statistical significance. This result validates the ISCCP calibration technique for removing response degradations in the satellite sensors [7].

C. Intersatellite Comparisons

The radiometric normalizations done for ISCCP geostationary imager calibration were designed to scale the sensors' response to a common reference, derived from the AVHRR measurements, with the intent to eliminate intersatellite calibration biases. It follows that the lunar irradiance measurements should agree between the satellites to within the uncertainties of the following: the ISCCP absolute calibration, the errors in the measurements from images (discussed hereinafter), and the lunar model relative precision ($\sim$1% [12]). In their evaluation of ISCCP radiance calibrations, Brest *et al.* [7] concluded that the mean relative uncertainty in the VIS-channel calibration was no larger than 3%–5% and the mean absolute uncertainty was about 10%, although later analyses have indicated that the latter number is too high [17].

With the determination that any actual sensor response drifts have effectively been removed by the ISCCP calibrations, the lunar measurement/model comparison series for each satellite can be considered a distribution of normalized radiometric measurements and statistical analysis applied. This provides an evaluation of cross-platform consistency. Table II gives the mean values and standard deviations of the irradiance comparison distributions for each satellite series, including both methods used for pixel radiance conversion.

TABLE II
STATISTICS ON LUNAR IRRADIANCE MEASUREMENT/MODEL COMPARISONS FOR ISCCP GEOSTATIONARY SATELLITES

Satellite	Pixel Radiance Conversion Method			
	Space-view Mean (Eq. 2)		Slope-intercept (Eq. 3)	
	Mean Comparison δ (%)	Standard Deviation	Mean Comparison δ (%)	Standard Deviation
GOES–6	-16.7	7.7	8.3	16.0
GOES–7	-15.6	8.1	9.4	17.1
GOES–8	3.3	3.5	-20.7	14.2
GOES–9	-3.1	2.8	-13.7	8.7
GOES–10	5.0	3.4	2.4	9.9
GOES–11	6.6	4.9	1.9	18.0
GOES–12	8.3	3.3	-21.1	18.6
GMS–3	-0.1	9.0	1.8	8.0
GMS–4	-7.4	5.6	-5.5	21.6
GMS–5	12.7	6.1	61.1	25.4

The current results, where (2) has been applied, indicate discrepancies in satellite-measured lunar irradiance of up to 17% (GOES-6) and overall discrepancies of about 8%. However, presuming an average lunar disk reflectance of 0.11 (typical for near full moon at 550 nm—this quantity is strongly dependent on phase angle and wavelength), the discrepancies in overall absolute reflectance amount to 1%–2%.

Nearly all the satellites show substantial differences between the two pixel radiance conversion methods. Since the image processing operations were identical in each case and the same ISCCP calibration slope is used in each method, these offsets must be attributed to the differences in background-level evaluations, either the mean of space-view pixel counts or the ISCCP calibration intercept. The larger differences (about 15% overall but $\sim$50% for GMS-5) seen using the ISCCP slope–intercept form (3) prompted further examination of the ISCCP radiance calibration procedure with particular attention given to the specification of the zero point (intercept) of the radiance regressions. No specific error source could be identified from this investigation. The scatter exhibited in the lunar comparisons in Figs. 2–4 suggests that this error might be an intrinsic limit to the precision of the ISCCP procedures for normalizing the geostationary satellite radiances to those of the concurrent AVHRR and then normalizing the concurrent AVHRR back to the reference NOAA-9 AVHRR.

D. ISCCP Geostationary Calibration

To develop a quantitative assessment of ISCCP geostationary sensor calibration from the current lunar analysis, corrections to the calibration intercept were derived which bring the measured lunar irradiances into agreement with the lunar model predictions. Table III lists these multiplicative correction factors for the satellites used in this study, given as the mean correction over all Moon observations in each satellite series. Because these corrections apply to the intercept only, the relative effect on the pixel radiance conversions over the full 8-b count range diminishes rapidly with increasing count values. Nonetheless, these factors represent a quantitative evaluation of this aspect of ISCCP calibration, referenced against the lunar model standard.

For the sensors with quadratic response functions (GOES-6 and GOES-7 and the GMS satellites), regression on the square of count values leads to significantly less well-constrained

TABLE III
STATISTICAL CORRECTIONS FOR ISCCP CALIBRATION INTERCEPTS

Satellite	Intercept Correction (Multiplicative Factor) Mean Correction	Standard Deviation
GOES–6	3.37	11.0
GOES–7	-6.68	34.3
GOES–8	0.82	0.12
GOES–9	0.83	0.07
GOES–10	1.07	0.12
GOES–11	1.04	0.22
GOES–12	0.84	0.14
GMS–3	0.61	1.35
GMS–4	0.80	1.47
GMS–5	-0.51	0.64

TABLE IV
COMPUTED ZERO-RADIANCE SENSOR RESPONSE LEVELS

Satellite	Mean Zero-radiance Response (CT) ISCCP Calibration (Eq. 3)	Eq. 3 with Incpt Correction	Space-view Pixel Level
GOES–6	4.27	12.9	26.1
GOES–7	(-393)	(-266)	7.86
GOES–8	8.97	7.27	6.97
GOES–9	8.01	6.58	6.92
GOES–10	6.99	7.44	6.96
GOES–11	7.50	7.54	6.99
GOES–12	9.39	7.77	6.99
GMS–3	(-27)	3.32	8.12
GMS–4	(-49)	(-100)	6.33
GMS–5	(-1200)	21.1	0.00

Note: values in parentheses are CT^2 in Eq. 3, see text.

intercept determinations. This explains the relatively large corrections found for these sensors. For the linear response satellites, the corrections to the intercepts are equivalent to only few counts.

As an additional diagnostic, Table IV provides three quantities related to the sensors' response to a zero-radiance input: the mean count values determined by solving the ISCCP calibration expression (3) for $L_i = 0$, the corresponding values computed with the intercept corrections applied, and the mean of space-view pixels (in CT) extracted from the lunar image subframes. It is important to note that the values listed in these tables were generated statistically from the series of observations and are not suitable for use for any ISCCP data processing. In some cases for the sensors with quadratic response functions, the radiance regressions have produced intercept values greater than zero, which gives nonreal roots for (3) with $L_i = 0$. For these instances, the mean counts-squared (CT^2) values are given in parentheses in the table.

V. UNCERTAINTY ASSESSMENTS

Because the ISCCP calibrations were found to have negligible temporal trends, the lunar observation series for each satellite, taken as comparisons against the irradiance model, can provide useful statistics for error analysis. For clarity, the data points in Figs. 2–4 have been plotted without error bars; however, the individual points carry uncertainty contributions from both the measured and modeled lunar irradiances. The magnitudes of these errors are discussed here.

A. Lunar Model Predictions

The USGS lunar model generates lunar irradiances with a relative accuracy $< 1\%$ over its full range of geometric variables. This precision derives from the model's construction by fitting thousands of radiometric measurements of the Moon acquired over many years at a dedicated observatory, covering a wide range of phase angles and lunar libration states. The model analytic form was developed empirically, with the driving objective being minimizing the residuals of the fit. Details of the model development are found in [12]. The $< 1\%$ predictive precision has been evaluated from the mean absolute fit residual. Although this uncertainty is systematic for a particular phase and libration state, it becomes a random error for the irradiance comparisons in Figs. 2–4 due the happenstance geometry of these chance observations.

The absolute radiometric scale of the USGS model cannot be verified at better than $\sim$5%, primarily due to uncertainties in measurements of its absolute calibration reference, the star Vega. The major source of this error comes from the observational data set on which the model is based having been acquired with ground-based telescopes, thus requiring atmospheric transparency corrections for the absolute calibration measurements. However, the model absolute error can only impose a systematic scale offset that is identical for all observations from a particular satellite. Furthermore, because the geostationary VIS channels in this study have quite similar spectral response functions, the absolute offset will be correspondingly similar for all the satellites. The lunar comparison results in Section III-B show that any such systematic bias has been masked by the much larger uncertainties in the lunar irradiance measurements from images.

B. Lunar Irradiance Measurements From Image Data

The uncertainty in irradiance measurements computed by (1) can be attributed to two sources: the pixel summation process and the calibrations used to convert the image pixels to radiance. Uncertainties in the ISCCP geostationary VIS-channel calibration are discussed in Section V-C.

Standard production of ISCCP B1 data spatially resamples VIS-channel images from a resolution of 0.9–2.5 km to approximately 10 km [13], which also removes any oversampling. For extended fairly homogeneous targets such as clouds, the error introduced by this process is negligible. However, because the Moon has a highly nonuniform distribution of reflectances over its surface, subsampling that removes interspersed pixels must affect the results of the pixel summations to some extent.

Fig. 6 shows comparison results for Moon image processing from full-resolution and ISCCP B1 image data. The two image extracts are from the same GOES-12 observation, with the subframes chosen to match as closely as possible. The full-resolution data, obtained from NOAA's Comprehensive Large Array-Data Stewardship System, have 10-b depth, requiring adjustments to the ISCCP calibration slope (a multiplicative factor of four) and the space-level threshold for on-Moon pixel selection. Increased precision is expected for irradiance measurements from full-resolution images, due to both the 10-b

Full Resolution

ISCCP B1 Reduced Resolution

	Full Resolution	ISCCP B1
Full-Earth Image Size	20836×10820	1172×1353
Moon Subframe Size	1600×600	100×75
Pixels on Moon	109802	887
Irradiance (μW/m^2 nm)	2.938	2.906

Fig. 6. GOES-12 lunar image acquired on November 10, 2008, at 14:45 UTC and comparison of Moon image processing and lunar irradiance measurement parameters for native-resolution and ISCCP B1 reduced-resolution images. The B1 subsampling factors are 1/16 and 1/8 in the sample and line dimensions, respectively.

data depth and the inclusion of ∼124 times more pixels (nominally 128) in the summation. The measured lunar irradiance was found to be ∼1.1% lower for the B1 reduced-resolution image. Similar comparisons on other GOES-12 images show this to be a typical result. This difference value is considered a contribution to the systematic uncertainty in the lunar irradiance measurements from ISCCP image data.

C. ISCCP Radiance Calibration

Quantitative uncertainties in the ISCCP geostationary VIS-channel calibration are considered to be no larger than 3%–5% relative and ∼10% absolute [7]. The ISCCP calibration procedure for geostationary satellites produces independent calibrations on a monthly basis, underpinned by the assumption of a consistent global climatology [6]. Any error in the anchor (NOAA-9) AVHRR absolute calibration constitutes a systematic error in the successor and predecessor AVHRRs that provide the references for the geostationary calibrations, but this will be identical for all the satellites used in this study.

Within the uncertainty limits described previously, the results of this study can be used to form an evaluation of uncertainty in the ISCCP radiance calibrations in the context of the lunar data comparisons. The monthly ISCCP calibration updates mean that uncertainty evaluations for each lunar observation are feasible, since individual radiance conversion factors have been applied to them. However, a statistical treatment for each satellite provides a more informative analysis.

The radiance conversion expression in (3) gives the ISCCP calibration in terms of a sensor "gain," represented by the calibration slope S_a, and a zero-level offset as the intercept I_a. For the current analysis, the slope is presumed to be well constrained by the calibration radiance regressions (cf. Section I and [6]). The intercept corrections that align the lunar irradiance measurements with the model results, discussed in Section IV-D, were developed from statistics on the series of Moon observations from each satellite, taken as a distribution of measurements. The standard deviations of these corrections provide a measure of the level of uncertainty, or imprecision, in the determinations of the calibration intercepts from the radiance regressions. These standard deviation values are given in Table III.

VI. Conclusion—Findings and Recommendations

This study has developed an assessment of ISCCP radiometric calibrations for geostationary imagers by comparison of observational data against a known external reference, the Moon. The analysis has demonstrated long-term temporal stability of the ISCCP calibrations for the GOES and GMS satellites used here.

Our results show relatively large differences in the sensors' response to the Moon in some cases, but these differences amount to only a few percent in measured absolute reflectances. There also is significant scatter in these results within each satellite series. Although the range of scatter generally falls within the expected uncertainty of ISCCP absolute calibration, this scatter is reduced if the image background level is either held constant or determined from space-viewing portions of the images. The much larger scatter seen using the ISCCP slope–intercept form for the pixel radiance conversion suggests a need for further investigation of the ISCCP normalization procedures for geostationary satellites.

The lunar images utilized in this study were captured by chance, i.e., by coincidence of the Moon's position in its orbit and the timing of geostationary imaging. Although favorable geometries occur over several geostationary orbits each month, only three to four usable lunar images per year were found from these chance encounters, partly as a result of the ISCCP 3-h sampling interval. This is too low a frequency to develop reliable calibration updates using the lunar method alone. We therefore recommend that all meteorological satellite operators acquire dedicated observations of the Moon at least monthly. The times and locations of Moon appearances can be predicted accurately far in advance. Since November 2005, NOAA has conducted regular observations of the Moon with the GOES East and West satellites, and lunar images were acquired during postlaunch testing for the three most recent GOES satellites (GOES-13, GOES-14, and GOES-15).

It was not possible to apply the lunar calibration technique to any ISCCP Meteosat or MTSAT data, because the off-Earth pixels, where the Moon would appear, were nulled in the B1 images. Our second recommendation is to keep these regions intact for low-processing-level image data (in fact, this was the original ISCCP request to the satellite agencies providing the data), not only to preserve images of the Moon but also to permit use of the image background to help anchor the calibration.

Although the primary absolute calibration for ISCCP data is tied to the AVHRR instruments on NOAA polar-orbiting satellites, coincident and collocated radiance regressions also have been generated for Moderate Resolution Imaging Spectroradiometer (MODIS) imaging [18], [19]. Cross-calibration of MODIS and AVHRR provides an important supporting connection to ISCCP calibration. The existing capabilities of lunar calibration enable the Moon to be utilized as a common reference for such cross-calibrations, and both MODIS and AVHRR have viewed the Moon. Realizing a lunar cross-calibration between these instruments is a recommended further step, but this exceeds the scope of the ISCCP calibration review project that included this lunar study.

Production of the multiyear global ISCCP radiance data set from the extensive collection of geostationary and polar-orbit meteorological images represents a pioneering effort toward development of a climate data record. The central issues of data interoperability and consistent calibration across multiple satellites have been the drivers for the development of ISCCP calibration procedures. Although these efforts have achieved a standardization of calibration for the meteorological satellites participating in ISCCP, it is widely recognized that reliable detection of climate change requires further reduction in calibration uncertainties. The current study has developed an independent evaluation of ISCCP calibration accuracy through application of lunar calibration techniques. The results have revealed apparent intersatellite calibration biases that were effectively masked by the ISCCP procedures, although the errors determined in the ISCCP calibration intercept, including both biases and random variations, appear to be within the estimated uncertainty in terms of absolute radiances. This has reinforced the need to utilize multiple pathways and techniques to assure stable and consistent calibration. We conclude that confirmation of such calibration interconsistency is a requirement to demonstrate quality assurance for data sets intended for climate applications.

ACKNOWLEDGMENT

The authors would like to thank K. Knapp at the National Climatic Data Center, National Oceanic and Atmospheric Administration, for providing the B1 unified image data used in this study.

REFERENCES

[1] R. A. Schiffer and W. B. Rossow, "The International Satellite Cloud Climatology Project (ISCCP): The first project of the world climate research program," *Bull. Amer. Meteorol. Soc.*, vol. 64, no. 7, pp. 779–784, Apr. 1983.

[2] C.-C. Liu, A. Kamei, K.-H. Hsu, S. Tsuchida, H.-M. Huang, S. Kato, R. Nakamura, and A. Wu, "Vicarious calibration of the Formosat-2 remote sensing instrument," *IEEE Trans. Geosci. Remote Sens.*, vol. 48, no. 4, pp. 2162–2169, Apr. 2010.

[3] K. J. Thome, K. Arai, S. Tsuchida, and S. F. Biggar, "Vicarious calibration of ASTER via the reflectance-based approach," *IEEE Trans. Geosci. Remote Sens.*, vol. 46, no. 10, pp. 3285–3295, Oct. 2008.

[4] Y. M. Govaerts, M. Clerici, and N. Clerbaux, "Operational calibration of the Meteosat radiometer VIS band," *IEEE Trans. Geosci. Remote Sens.*, vol. 42, no. 9, pp. 1900–1914, Sep. 2004.

[5] C. L. Brest and W. B. Rossow, "Radiometric calibration and monitoring of NOAA AVHRR data for ISCCP," *Int. J. Remote Sens.*, vol. 13, no. 2, pp. 235–273, Jan. 1992.

[6] Y. Desormeaux, W. B. Rossow, C. L. Brest, and G. G. Campbell, "Normalization and calibration of geostationary satellite radiances for the international satellite cloud," *J. Atmos. Ocean. Technol.*, vol. 10, no. 3, pp. 304–325, Jun. 1993.

[7] C. L. Brest, W. B. Rossow, and M. D. Roiter, "Update of radiance calibrations for ISCCP," *J. Atmos. Ocean. Technol.*, vol. 14, no. 5, pp. 1091–1109, Oct. 1997.

[8] E. A. C. H. Whitlock, "AVHRR and VISSR Satellite Instrument Calibration Results for Both Cirrus and Marine Stratocumulus IFO Periods," NASA, Washington, DC, FIRE Sci. Rep. CP 3083, 1990.

[9] C. R. N. Rao, J. Chen, F. W. Staylor, P. Able, Y. J. Kaufman, E. Vermote, W. B. Rossow, and C. Brest, "Degradation of the Visible and Near-Infrared Channels of the Advanced Very High Resolution Radiometer on the NOAA-9 Spacecraft," NOAA, Silver Spring, MD, Tech. Rep. NESDIS 70, 1993.

[10] C. R. N. Rao and J. Chen, "Inter-satellite calibration linkages for the visible and near-infrared channels of the Advanced Very High Resolution Radiometer on the NOAA-7, -9, -11 spacecraft," *Int. J. Remote Sens.*, vol. 16, no. 11, pp. 1931–1942, Jul. 1995.

[11] P. Abel, B. Guenther, R. N. Galimore, and J. W. Cooper, "Calibration results for NOAA-11 AVHRR channels 1 and 2 from congruent path aircraft observations," *J. Atmos. Ocean. Technol.*, vol. 10, no. 4, pp. 493–508, Aug. 1993.

[12] H. H. Kieffer and T. C. Stone, "The spectral irradiance of the moon," *Astronom. J.*, vol. 129, no. 6, pp. 2887–2901, Jun. 2005.

[13] R. A. Schiffer and W. B. Rossow, "ISCCP global radiance data set: A new resource for climate research," *Bull. Amer. Meteorol. Soc.*, vol. 66, no. 12, pp. 1498–1505, Dec. 1985.

[14] K. R. Knapp, "Scientific data stewardship of International Satellite Cloud Climatology Project B1 global geostationary observations," *J. Appl. Remote Sens.*, vol. 2, no. 1, p. 023 548, Nov. 2008.

[15] W. B. Rossow, A. Walker, and M. Roiter, "International Satellite Cloud Climatology Project (ISCCP) Description of Reduced Resolution Radiance Data," World Climate Res. Programme, Geneva, Switzerland, Tech. Rep. WMO/TD-58, 1996.

[16] H. H. Kieffer, "Photometric stability of the lunar surface," *Icarus*, vol. 130, no. 2, pp. 323–327, Dec. 1997.

[17] Y. Zhang, W. B. Rossow, A. A. Lacis, V. Oinas, and M. I. Mischenko, "Calculation of radiative fluxes from the surface to top of atmosphere based on ISCCP and other global data sets: Refinements of the radiative transfer model and the input data," *J. Geophys. Res.*, vol. 109, no. D19, p. D19 105, Oct. 2004.

[18] A. K. Heidinger, W. C. Straka, C. C. Molling, and J. T. Sullivan, "Deriving an inter-sensor consistent calibration for the AVHRR solar reflectance data record," *Int. J. Remote Sens.*, vol. 31, no. 24, pp. 6493–6517, Jul. 2010.

[19] C. C. Molling, A. K. Heidinger, W. C. Straka, and X. Wu, "Calibrations for AVHRR channels 1 and 2: Review and path towards consensus," *Int. J. Remote Sens.*, vol. 31, no. 24, pp. 6519–6540, Dec. 2010.

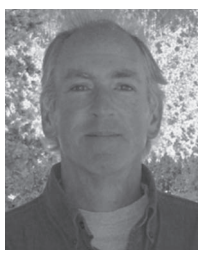

Thomas C. Stone received the Ph.D. degree in atmospheric science from The University of Arizona, Tucson, AZ, USA, in 1998.

He is currently with the Astrogeology Science Center, U.S. Geological Survey, Flagstaff, AZ, USA, where he leads the Lunar Calibration project Robotic Lunar Observatory (ROLO) to utilize the Moon as a radiometric reference source, primarily for on-orbit calibration of Earth remote sensing satellite instruments. Previously, he has worked with spaceflight instrumentation, e.g., the Miniature Integrated Camera Spectrometer UV spectrometer on Deep Space 1, the Imager for Magnetopause-to-Aurora Global Exploration-Extreme Ultraviolet imager, and a space-shuttle-based imaging spectrometer for studies of Earth's upper atmosphere, where his experience included instrument development, manufacture, calibration, and payload operations. His current research interests include advancing development of the lunar radiometric standard, applying lunar calibration techniques to archived image data from meteorological satellites for retrocalibration and cross-calibration, and enabling measurement of aerosol optical properties at night using the Moon as a light source.

William B. Rossow received the B.A. degree (*magna cum laude*) in physics/mathematics from Hanover College, Hanover, IN, USA, in 1969 and the M.S. degree in physics and the Ph.D. degree in astronomy from Cornell University, Ithaca, NY, USA, in 1972 and 1976, respectively.

Since September 2006, he has been a Distinguished Professor of Remote Sensing with The City University of New York, New York, NY, USA, where he is also with the CUNY Remote Sensing of Earth Institute. For the 28 years before that, he was a Physical Scientist with the Goddard Institute for Space Studies, National Aeronautics and Space Administration. Since 1982, he has been the Head of the Global Processing Center of the International Satellite Cloud Climatology Project for the World Climate Research Program. He conducts research on cloud physics and dynamics, atmospheric radiative transfer, atmospheric dynamics, and satellite remote sensing of Earth's climate and other planetary atmospheres. He has published over 230 papers and reports.

Dr. Rossow was a recipient of the NASA Exceptional Scientific Achievement Medal in 1988 and the American Meteorological Society Verner E. Suomi Award in 2005 and is a Fellow of the American Geophysical Union and the American Meteorological Society.

Joseph Ferrier received the B.S. degree in applied physics from Columbia University School of Engineering and Applied Sciences, New York, NY, USA, in 1980 and the M.S. degree in physics and astronomy from the Graduate School of Arts and Science, New York University, New York, NY, USA, in 1983.

He is currently with the Goddard Institute for Space Studies, National Aeronautics and Space Administration, New York, NY, USA, where he works on both visible and infrared calibration issues for the International Satellite Cloud Climatology Project. Previously, he was involved with calibration and data analysis of the PhotoPolarimeter experiment aboard the Galileo orbiter of Jupiter. He has also done image design and analysis of the Imaging Science Subsystem experiment for the Cassini Project, for both the flyby of Jupiter and the orbital mission of Saturn.

Laura M. Hinkelman received the Ph.D. degree in meteorology from The Pennsylvania State University, University Park, PA, USA, in 2003.

She was a Research Scientist with the National Institute of Aerospace, contracting with the Langley Research Center, National Aeronautics and Space Administration (NASA). She is currently a Research Scientist with the Joint Institute for the Study of the Atmosphere and Ocean, University of Washington, Seattle, WA, USA. Her research interests include the Earth's energy budget, long-term trends in surface insolation, and the effect of clouds on atmospheric radiative transfer. She has worked extensively with ground-based measurements and satellite retrievals of solar fluxes, Monte Carlo radiative transfer, and large-eddy simulation models. Her current projects focus on evaluating and applying measured radiation data. She collaborates in the evaluation of satellite-retrieved surface radiative fluxes for the NASA/GEWEX Surface Radiation Budget product. In addition, she leads a project testing the utility of using satellite radiation data as input to snowmelt models. Her most recent area of application is solar energy, where her projects focus on characterizing solar irradiance variability and its sources at small spatial scales. The aim of all her research is to improve our understanding of radiative transfer through the atmosphere and to apply this understanding to practical problems with societal relevance.